HHS Public Access

Author manuscript

J Pharm Sci. Author manuscript; available in PMC 2017 January 13.

Published in final edited form as:

J Pharm Sci. 2016 January ; 105(1): 147–159. doi:10.1016/j.xphs.2015.11.027.

Current Inhalers Deliver Very Small Doses to the Lower Tracheobronchial Airways: Assessment of Healthy and Constricted Lungs

Ross L. Walenga[1] and **P. Worth Longest**[1,2,*]

[1]Department of Mechanical and Nuclear Engineering Virginia Commonwealth University, Richmond, VA

[2]Department of Pharmaceutics Virginia Commonwealth University, Richmond, VA

Abstract

To evaluate the regional delivery of conventional aerosol medications, a new whole-lung computational fluid dynamics (CFD) modeling approach was applied for metered dose inhaler (MDI) and dry powder inhaler (DPI) aerosols delivered to healthy and constricted airways. The CFD approach included complete airways through the third respiratory bifurcation (B3) and applied the new stochastic individual pathway (SIP) modeling technique beyond B3 through the remainder of the conducting airways together with a new model of deposition in the alveolar region. Bronchiolar (B8-B15) deposition fraction (DF) values were low (~1%) for both MDI and DPI aerosols with the healthy geometry, while delivery to the constricted model was even lower, with DF values of 0.89% and 0.81% for the MDI and DPI, respectively. Calculating dose per unit-surface-area for the commercial MDI and DPI products resulted in approximately 10^{-3} μg/cm^2 in the lower tracheobronchial (TB) region of B8-B15 and 10^{-4} μg/cm^2 in the alveolar region. Across the lung, dose per unit-surface-area varied by 2 orders of magnitude, which increased to 4 orders of magnitude when the mouth-throat region was included. The MDI and DPI both provided very low drug dose per unit-surface-area to the small TB and alveolar airways.

Keywords

airway constriction; asthma; metered dose inhaler; dry powder inhaler; whole-lung CFD model; respiratory drug delivery; small airways

[*]**Author Contact Information:** (Corresponding author), Virginia Commonwealth University, 401 West Main Street, P.O. Box 843015, Richmond, VA 23284-3015, Phone: (804)-827-7023, Fax: (804)-827-7030, pwlongest@vcu.edu.
Dr. Ross L. Walenga, PhD, Virginia Commonwealth University, 401 West Main Street, P.O. Box 843015, Richmond, VA 23284-3015, Phone: (804)-827-7023, Fax: (804)-827-7030, walengarl@vcu.edu

Author Disclosure Statement

No conflicts of interest exist.

Introduction

Airway inflammation leading to lumenal wall narrowing, i.e., constriction, is a characteristic of multiple respiratory diseases including asthma and chronic obstructive pulmonary disease (COPD).[1-4] Considering asthma, inflammation associated airway wall thickening can be identified at all levels of the lungs, including the small airways.[1,2] For example, Hamid et al.[2] measured inflammatory cell counts in cryosectioned lung tissue from asthmatic (n = 6) and non-asthmatic (n = 10) subjects following a lung resection procedure, and results showed that for asthmatic patients, activated eosinophil counts were higher in the peripheral airways (< 2 mm internal perimeter) as compared with the central airways (> 2 mm internal perimeter), while counts of other inflammatory cell types (T cells, total eosinophils, mast cells) showed no significant difference. Airway dimensions were measured by Carroll et al.[5] from *ex vivo* subjects, all of whom had died suddenly. This patient population included subjects where asthma was the cause of death (n = 11), a history of asthma was present but was not identified as the cause of death (n = 13), and no history of asthma was present (n = 11).[5] The small membranous bronchiole (perimeter < 2 mm) measurements showed the total and outer wall areas were larger for all asthma cases as compared with the control, which would reduce the airway lumenal area available for airflow.[5] Changes in central and peripheral airway resistance measured using a micromanometer showed that for asthma patients with constricted airways (n = 10), peripheral resistance as a percentage of total resistance increased from a healthy control value of 24 ± 6% to 51 ± 6% ($p < 0.01$).[6] Kuwano et al.[7] measured peripheral airway dimensions *ex vivo* from patients with fatal asthma, non-fatal asthma, and chronic obstructive pulmonary disease (COPD), as well as normal subjects. It was observed that wall thickening was greater for fatal asthma subjects than for non-fatal asthma subjects, and it was suggested that the hyper-responsiveness in the small airways noted by Wiggs et al.[8] may play a role in the severity of asthma and ultimately whether or not it proves to be fatal.[7] Moreover, an increased peripheral airway constriction has been noted in children compared with adults.[1,3,9]

Uncontrolled asthma is a significant issue, affecting approximately greater than half of all asthma patients.[10-12] For these cases, new medications appear to be needed, and while the type of medication is often the target for development, delivery efficiency to the affected regions of the lungs is also important. It is well known that particle size is a large factor in controlling where aerosols deposit in the lungs. Most commercially available metered dose inhalers (MDIs) or dry powder inhalers (DPIs) deliver a majority of the aerosol size distribution as large particles (> 2 μm), which are typically filtered upstream in the extrathoracic and large airway regions due to impaction and turbulent dispersion. A series of *in vivo* studies showed that monodisperse albuterol sulphate particles with diameters of 3 and 6 μm more effectively targeted the large airway region as opposed to a 1.5 μm aerosol, which deposited preferentially in the small airways.[13-15]

The effect of decreased drug delivery to the small airways with conventionally sized aerosols is exacerbated by the fact that the surface area of the airways increases exponentially with depth into the lungs. Estimates of large and small airway surface area may be found based on the convention in the literature that large airway diameters are typically ≥ 2 mm and small airway diameters are < 2 mm.[1,16-18] Using the anatomical

measurements of Yeh and Schum[19] for an adult and scaling to a lung volume of 3.5 L,[20] large and small airway surface areas are calculated as 0.1 m^2 and 62.8 m^2, respectively. These estimates include the alveolar region as part of the small airways, which accounts for 62.6 m^2. Lung response to surface active medications most likely occurs on the basis of dose per unit-surface-area. The extremely large surface area of the small airways may therefore result in doses that are too low to achieve the desired therapeutic effect. As described above, inflammation associated with asthma affects the airways from the upper tracheobronchial (TB) region through the alveoli.[2,21,22]

Some small-particle aerosol medications for treating asthma have already been introduced. As part of the switch from chlorofluorocarbon (CFC) to hydrofluoroalkane (HFA) 134a propellant in MDIs as specified by the Montreal Protocol, small-particle corticosteroid inhalers have been developed for ciclesonide and beclomethasone dipropionate, which have been shown to increase total lung deposition and bronchiolar airway drug delivery.[10,23-25] Recently, Bulac et al.[26] assessed patient response (n = 95) to a beclomethasone dipropionate/formoterol HFA MDI formulation with a mass median aerodynamic diameter (MMAD) of approximately 1.5 μm (based on cascade impaction)[27] compared to regular maintenance therapy, and reported that the smaller particle size produced a significant improvement in exhaled nitric oxide and ventilation heterogeneity in the acinar region associated with a reduction in small airway inflammation. However, while the change from CFC to HFA 134a when combined with ciclesonide and beclomethasone dipropionate reduces the aerosol aerodynamic size to approximately 1.1 μm,[23] other drugs such as fluticasone propionate do not experience a size reduction,[28] so small airway drug delivery with those medications is still a significant concern. Furthermore, most current DPI products produce conventionally sized aerosols with relatively large MMADs, especially when the fraction that deposits in the preseparator during cascade impaction testing is included in the size calculation.[29-31] For example, the Flovent Diskus DPI (GlaxoSmithKline, Raleigh, NC) delivering 250 μg of fluticasone propionate produces MMADs of 2.99 μm and 4.10 μm when tested at flow rates of 75 and 45 LPM (L/min),[30] respectively, using standard cascade impaction procedures and excluding the preseparator deposited mass, which is standard practice. Including the preseparator deposited mass in the size distribution, which the patient inhales during aerosol delivery, can easily double or triple the reported MMAD value.[29]

The primary purpose of this study was to characterize bronchial and bronchiolar airway deposition of two commercially available MDI and DPI aerosol products, which both deliver fluticasone propionate with an MMAD of approximately 3 μm. This aerodynamic particle size is expected to be effective for deep lung penetration of the aerosol.[32-34] Analysis of regional and local airway deposition throughout the lungs is based on the newly developed stochastic individual pathway (SIP) modeling approach[31,35] and CFD-based alveolar deposition predictions.[36] Application of CFD modeling with the SIP approach is expected to capture the drug dose received by the important bronchiolar airways in a manner that is not possible with lung deposition correlations[37,38] and *in vivo* imaging techniques.[39] Based on previous regional deposition CFD studies, it is expected that very low doses of the inhaled medication are actually deposited in the bronchiolar airways.[29] However, actual drug deposition values per unit-surface-area in the lung have not previously been reported for

pharmaceutical aerosols from realistic whole-lung CFD simulations. Furthermore, this study will evaluate the effect of inflammation associated constriction on regional deposition fraction and dose per unit-surface-area. Several studies have previously used CFD methods to characterize aerosol deposition in asthma constricted patients,[33,40-45] but whole-lung CFD simulations have not previously been implemented for this diseased lung state. Considering that inflammation associated with asthma occurs at all levels of the lung including the alveolar region,[1,2,5,46] ideal drug delivery of anti-inflammatories like fluticasone propionate should provide a relatively uniform dose per unit-surface-area throughout the airways to be most effective. In contrast, dose per unit-surface-area values that differ by several orders of magnitude throughout the lung may indicate poor targeting of the medication.

Materials and Methods

Airway definitions

Clinical and biological studies often delineate the large airways as having diameters ≥ 2 mm and small airways as having diameters < 2 mm.[1,16-18] However, airway diameter and the related classification between large and small airways is subject to change as a function of the respiratory cycle, or in the case of anatomical research studies, the casting or fixation techniques that are applied to the lungs.[19,47-49] In contrast, ICRP[20] defines bronchi as containing some cartilage and glands and extending from respiratory generation G0 (trachea) to G8. Bronchioles do not contain cartilage or glands and extend from G9 through the terminal bronchioles at G15, which lead to the alveolar region.[20] In the current study, TB airways are classified in a manner similar to ICRP,[20] but on the basis of bifurcations instead of generations. The advantage of working with bifurcations is that the important carinal region is included without the need for additional definitions, which are frequently different among the available anatomical studies.[16,49,50] To remain consistent with previous bifurcation-based lung models and whole-lung CFD simulations, B1-B3 (trachea to lobar bronchi) is the upper TB region, B4-B7 is the middle TB region, and B8-B15 is the lower TB region. In comparison to ICRP,[20] B1-B7 represents the bronchi and B8-B15 represents the bronchioles. For comparisons with previous anatomical studies, the ”small TB airways” with diameters < 2 mm are approximately B13-B15 (see Table 1); and the ”small airways” are B13-B15 together with the alveolar region.

Inhalers

The MDI and DPI devices selected were Flovent HFA MDI and Flovent Diskus DPI (both from GlaxoSmithKline, Raleigh, NC). The aerosolized dose from both inhalers is 250 μg of fluticasone propionate. The emitted dose of the Flovent HFA MDI is 220 μg, which indicates an estimated 12% loss within the device. In the MDI, micronized fluticasone propionate is suspended without any additional excipients in HFA 134a and has a total metered mass (propellant plus drug) of 75 mg per actuation. Micronized fluticasone propionate is blended with lactose in the Flovent DPI with a total dose mass of 12.5 mg. Previously, our group has conducted *in vitro* experiments that characterized the size distribution and deposition characteristics of aerosols emitted from these inhalers under different typical airflow conditions.[30,31] For a typical MDI inhalation flow rate of 30 LPM, the Flovent HFA MDI aerosol had an MMAD of 2.64 μm with a standard deviation of 0.1

and a geometric standard deviation (GSD) of 1.51. The typical mean inhalation flow rate of the Flovent Diskus DPI is 75 L/min, which produced an MMAD of 2.99 μm with a standard deviation of 0.2 and a GSD of 2.09.[30,31]

Healthy and asthmatic lung models

For this study, the previously developed mouth-throat (MT)[51] and tracheobronchial (TB)[31] models were used to create non-constricted and constricted airways with MDI and DPI mouthpieces, as illustrated in Figure 1. The TB airway dimensions were outlined by Tian et al.[31] and are based on the anatomical cast data of Yeh and Schum[19], which are then scaled to a lung volume (3.5 L) representative of an average adult male while using an inhaler.[20] Based on the previous airway model development study of Walenga et al.,[52] the upper TB model which includes the trachea through the third respiratory bifurcations (B1-B3) is referred to as Model C. Heistracher and Hofmann[53] published physiologically realistic bifurcation (PRB) parameters that were used to design the bifurcation units for Model C together with the anatomical dimensions from Yeh and Schum,[19] though some modifications to the PRB units were necessary to facilitate smooth asymmetrical branching. The branch radii of curvatures and the carinal ridge features were adopted from the measurements of Hammersley and Olson[54] and Horsfield et al.[50] The branch gravity angles reported by Yeh and Schum[19] were utilized to define bifurcation unit rotations. Since the TB airways terminated at the third bifurcation level, each lobe had one inlet bifurcation, with the exception of the right lower and middle lobes, which had one inlet branch. Using measurements from the *ex vivo* study of Russo et al.[55] and other collected CT scans, a D-shaped tracheal cross section was formed and cartilaginous rings were added to the Model C trachea.[31]

In this study, inflammation induced airway constriction is evaluated by homogenously reducing the airway diameters but not the airway lengths. This form of airway constriction is associated with the long-term process of airway remodeling which occurs in asthma at all levels of the conducting airways in response to the ongoing inflammatory process.[7,56-59] Previous studies have reported non-fatal asthma associated reductions in airway diameter due to remodeling in the range of 10-100%.[7,56,60] In this study, a 30% diameter reduction was used as a conservative estimate to capture the long-term inflammation-induced process of remodeling. Because the remodeling response is reported to occur throughout the conducting airways,[2,7,59] the 30% diameter reduction was uniformly applied beginning with the trachea and extending to the terminal bronchioles (B15). Furthermore, a uniform degree of airway constriction associated with remodeling was not expected to largely influence the lobar ventilation distribution. In contrast, an acute asthma attack is associated with highly heterogeneous lung constriction and will significantly affect the lobar ventilation distribution.[46] Therefore, the current model is intended to capture the effect of long-term airway remodeling associated with asthma[59] but not bronchoconstriction associated with acute smooth muscle cell contraction[46] during an asthma attack.

As described by Tian et al.[31,35] and Longest et al.,[30] the airways from the fourth bifurcation (B4) to the fifteenth bifurcation (B15) were modeled using the SIP approach. Five SIP models were scaled by Longest et al.[30] to simulate flow and particle transport into the five

lung lobes of non-constricted models for MDI and DPI delivery. As described above, constricted versions of the five SIP models were constructed by applying a 30% diameter reduction in the same manner as with the upper TB airway models in Figure 1 in order to capture inflammation associated airway remodeling. The five SIP models are designated as the left lower (LL), left upper (LU), right lower (RL), right middle (RM), and right upper (RU) lobar paths for the nonconstricted and constricted cases. The LL, LU, and RU pathways begin at the third bifurcation (B3), but the RL and RM pathways begin at B4 and are unique. Non-constricted and constricted versions of the LL model are shown in Figure 2, while the other models which are similar in appearance are not pictured. The average diameters of the SIP models, given in mm, are displayed in Table 1. The RL SIP model is based on dimensional data from Yeh and Schum[19] and scaled to represent a lung volume of 3.5 L, as described by Tian et al.,[31] while the four other SIP models are scaled from the RL SIP model to match the lobar outlets of Model C.

The computational meshes for the non-constricted versions of the upper TB airways were identical to those used in Walenga et al.,[52] with ~1×10^6 and ~1.4×10^6 cells used for the MDI and DPI models. The constricted models were constructed in the same manner, while the near-wall cell heights were based on the same gradient used in the non-constricted models, which resulted in smaller cell heights near the wall. This mismatch of near-wall cell heights has been known to cause discrepancies in Lagrangian particle tracking corrections due to drag and turbulence, and in this study the user defined functions (UDFs) used for these corrections were updated to avoid this issue, as described later in this section. The y^+ values of each constricted case were checked and were found to be similar to those from the non-constricted cases. The numerical extensions at the upper TB bifurcation outlets were omitted to allow for interpolation of flow field and particle tracking information to the SIP models.

The non-constricted and constricted SIP meshes were constructed with GAMBIT 2.4 (ANSYS, Inc., Canonsburg, PA, USA) using hexahedral elements in the same manner as the upper TB meshes. Two versions of each SIP model were constructed, one with numerical extensions at the outlets to avoid the development of unrealistic turbulence, and the other without to allow for a more realistic pressure distribution at the outlets, since it was unknown which would have a greater effect on particle deposition. Since the models were split between B4-B7 and B8-B15, the numerical extension at B7 was omitted in both cases to allow for interpolation of flow and particle data. The meshes from B4-B7 had approximately 2.4×10^5 and 1.8×10^5 cells with and without extensions, respectively, while the meshes from B8-B15 had approximately 4.2×10^5 and 3.0×10^5 cells with and without extensions, respectively. The work of Walenga[61] showed that the extensions were not necessary in the SIP models, leading to the use of meshes that excluded the extensions in this study.

Inhalation airflow waveforms and boundary conditions

The inhalation airflow waveforms of the MDI and DPI models were based on the study of Longest et al.[30] In that study, slow and deep (SD) and quick and deep (QD) transient inhalation waveforms were developed to represent correct patient usage boundary conditions

for the MDI and DPI, respectively. The waveforms were based on a 3 L inhaled volume for both the MDI and DPI, which was found to be consistent with the study of Broeders et al.,[62] and resulted in 37 L/min and 75 L/min mean flow rates for MDI and DPI inhalations, respectively. Other parameters reported by Longest et al.[30] were the peak inspiratory flow rate (PIFR) and the period of inhalation (T), which were found to be 61.4 L/min and 4.86 s for the SD profile and 122.2 L/min and 2.40 s for the QD profile. Longest et al.[30] considered both correct and incorrect inhalation profiles with MDI and DPI inhalers, but for this study only correct usage is considered. Specifically, the simulations with the MDI are conducted under transient conditions with the SD waveform, while the DPI predictions use the QD waveform.

The velocity inlet boundary conditions for the SIP predictions were interpolated from the B3 outlets at the time steps when the inhalation flow rates of the MDI and DPI simulations were at their mean accelerating values (i.e. 37 and 75 L/min, respectively). The SIP model simulations were run under steady state conditions for computational efficiency, which was previously justified in the study of Tian et al.[31] Moreover, it was necessary to split the models because the particle trajectory calculations would be nearly intractable as described later in this section using the SIP approach. Tian et al.[31] compared aerosol deposition predictions in three different RL lobe SIP models under steady state and QD conditions, and found differences in the regional deposition predictions to be less than 0.2%, indicating that the steady state approximation is adequate.

For all cases, an outflow ventilation distribution was specified at the upper TB outlets leading to each lung lobe, based on data from an analytical model[63] and two CT scans from a single human subject.[64] At these lobar outlets the following ventilation distribution was applied: LU 15%, LL 31%, RU 14%, RM 7%, and RL 33%. On a whole lung basis, the right and left lung ventilation values were 54% and 46%, respectively. It was assumed that ventilation was symmetrically distributed for all bifurcations past the lobar bronchi.

Flow field solution

Flow field simulations were conducted using ANSYS FLUENT 14.5 (ANSYS, Inc., Canonsburg, PA, USA). Many of the CFD simulation methods and boundary conditions for the conducting airway predictions were similar to those employed in other studies by our group.[30,31,35,52,65] The MDI simulations from the mouth-throat (MT) through B3 were turbulent, compressible, transient, and required both temperature gradient and species transport calculations. The temperature and concentration gradient calculations of the MDI were based on the methods of Longest and Xi[66] and Longest et al.[65] The DPI solutions in the MT and upper TB airways were based on turbulent, incompressible, transient and isothermal flow. Regarding the SIP models for both the MDI and DPI aerosols, the flow fields were modeled as turbulent, incompressible, isothermal, and steady state as indicated above. While these conditions were consistent with the DPI simulations in the upper TB region, they differed from the MDI simulations in the upper TB region but were located far enough away from the inlet jet that the density, temperature, and species concentrations were considered to be nearly constant. All simulations used the low Reynolds number (LRN) k–ω turbulence model, which has been shown to provide good predictions of

polydisperse particle transport and deposition for MDIs[65,67,68] and DPIs.[31] The outlet conditions for the upper TB model at B3 with the MDI simulations were specified using pressures at the boundaries that were obtained by first predicting flow with the mass-flow distribution specified previously in this section. Pressure outlets were necessary for the compressible MDI simulations, but not for the incompressible DPI simulations, which employed the mass-flow distribution directly. The SIP model outlets utilized symmetric mass-flow distributions.

Particle tracking

Particle trajectory calculations were performed using a Lagrangian particle tracking model, while turbulent dispersion was applied using a random walk method. Since particle size change was not considered, the effects of the particles on energy, mass, and momentum of the flow field were considered to be negligible and thus the discrete phase was modeled as one-way coupled. As described previously by Longest et al.[30], the evaporation of HFA in the MDI simulations has a very strong effect on the flow field and particle trajectories, and is captured through including HFA as a separate chemical species with a sonic inlet velocity condition at the MDI nozzle. The polydisperse particle distributions were the same that were used in Walenga et al.[52] for both the MDI and DPI predictions. Codes from ANSYS FLUENT 14.5 and custom UDFs were used to apply a near-wall correction to model anisotropic turbulence as implemented by Longest et al.,[65] since the LRN k–ω model uses a near-wall isotropic turbulence assumption that may over-predict aerosol deposition.[69] Additionally, a linear interpolation of near-wall velocities was applied in a similar fashion.

A key feature of this study was an adjustment to the near-wall drag and turbulence corrections for Lagrangian particle tracking. As described by Longest and Xi,[70] the particle trajectory calculations are updated using mean fluid velocities at each time-step, which are determined through interpolation from nodal values or control volume centers. However, Longest and Xi[70] found that fluid velocities at near-wall control volumes do not approach zero at the wall in the ANSYS FLUENT turbulent particle tracking code, and thus a linear interpolation of fluid velocities in the viscous sublayer for calculating particle trajectories was implemented using UDFs in combination with the commercial code, which in effect creates a first order approximation of the boundary layer between the first near-wall cell center and the wall. However, a disadvantage of this approach is that mesh density can affect deposition, since any alteration in the size of near-wall control volume heights may have an effect on particle deposition. For this reason, the fluid-velocity correction UDF was updated to be applied only when it is within a certain pre-defined near-wall limit (nw_{limit}), independent of its position in relation to near-wall cell volumes. Values of nw_{limit} were selected based on comparisons with *in vitro* data for the identical inhalers and non-constricted airway models considered in this study. The selected values ranged from 0.1 to 0.05 mm with variation between the maximum and minimum values based on linear scaling with changes in diameter associated with constriction and bifurcation number. Further details of the nw_{limit} specification and new UDF routine are available in Walenga.[61]

Turbulent particle dispersion was simulated throughout the conducting airways using an eddy interaction model. As previously described, the LRN k-ω model assumes directionally

independent turbulent fluctuations all the way to the wall, or isotropic turbulence.[65,67] The eddy interaction model was corrected to reduce the magnitude of wall normal turbulence fluctuations within a distance defined as the n^+_{limit}.[65,67,69,71] As with the calculation of the near-wall velocity, turbulent kinetic energy in the calculation of turbulent particle dispersion was interpolated in a mesh independent manner to allow for direct comparisons between the normal and constricted grids. Based on validations with *in vitro* data, described later in this section, a value of $n^+_{limit} = 60$ was used in all cases.

Particle positions at the B3 outlets (LL, LU, RL, RM, RU) of the upper TB model were recorded over the entire course of the transient upper airway simulations and were then injected into the inlets of the corresponding SIP models, in which steady state simulations were conducted. The polydisperse particle distribution at the B3 outlets from all of the Model C simulations consisted of ~3,000 particles, which were too few to provide an accurate characterization of the deposition efficiency in the lower regions of the SIP models, which extend from B4 to B15. Thus, the models were split into two sections from B4-B7 and B8-B15 in the same manner as Longest et al.[30] to reduce the number of particles necessary, which was estimated to be ~45,000 particles for the B4-B7 section and ~1,500,000 particles for the B8-B15 section. The fluid velocities and particle profiles at the outlets of the B4-B7 models were interpolated to the corresponding B8-B15 models. To provide the required number of particles for each SIP model, multiple copies of the inlet particle cross-sectional profile were simulated concurrently. The inclusion of turbulent dispersion modeling in the particle trajectory calculations ensured a unique path for each particle due to the randomness inherent in turbulent transport.

Comparison of CFD simulations with existing in vivo and in vitro data

A recent study from our group has successfully compared regional CFD predictions using the SIP modeling approach with *in vivo* deposition data for spray and dry powder inhaler aerosols throughout the lungs.[72] Specifically, Tian et al.[72] showed <10% relative error in deposition fraction (DF) predictions between the CFD results and *in vivo* data that characterized regional Novolizer DPI and Respimat softmist inhaler drug delivery. While successful comparisons with *in vivo* data are highly desirable, regional gamma scintigraphy lung imaging data with the Flovent HFA MDI and Flovent Diskus DPI were not available for this study, and so the *in vitro* data from Longest et al.[30] and Tian et al.[31] were used as a basis for model validation.

For comparisons with *in vitro* data in the current study, the inlet and outlet conditions of the MDI and DPI simulations were the same as those used in Walenga et al.,[52] where a transient inspiratory square wave was used with particle release during the first 0.2 s for the MDI aerosol, and a transient inspiratory square wave with a ramp-up from 0 to 0.05 s with a bolus of particles released at 0.025 s was used for the DPI aerosol. In both cases, the non-constricted model was used for validation. The only difference between the current validation and the previous study of Walenga et al.[52] was the updated treatment of near-wall corrections implemented in the current study, as described above. For the MDI validation, the resulting predictions of DF in the MT (including the mouthpiece - MP) and upper TB regions (B1-B3) were 50.3% and 0.6%, which showed good agreement with the *in vitro* data

of 49.7% and 0.6%, respectively. For the DPI validation, the predicted values of DF in the MT and upper TB regions were 72.0% and 2.3%, which showed good agreement with the *in vitro* data of 72.5% and 2.2%, respectively.

Deposition metrics

The amount of drug depositing in a given region may be expressed as either a fraction or as an efficiency. Based on the drug mass of the nominal dose, the deposition fraction (DF) for the *i*-th region is calculated as

$$DF_i = \frac{mass\ of\ drug\ depositing\ in\ region\ i}{initial\ mass\ of\ aerosolized\ drug} \quad (1).$$

The deposition efficiency (DE) for region *i* is calculated as

$$DE_i = \frac{mass\ of\ drug\ depositing\ in\ region\ i}{mass\ of\ drug\ entering\ region\ i} \quad (2).$$

The values of DF_i may be directly summed to provide predictions for larger regions. Deposition efficiency is a useful metric for assessing the probability of particle deposition in a given region separate from the influence of upstream effects. Similar to DF, the fraction remaining, FR_i, represents the fraction of the aerosolized dose remaining at the outlet in the *i*-th region.

Values of DF in the SIP models were evaluated on a regional basis from B4-B7, B8-B15, and B4-B15 using the DE values from the CFD predictions. In the same manner as Longest et al.[29] and ICRP,[20] the DE of the given region from the *i*th bifurcation to the *j*th bifurcation was first calculated as

$$DE_{region} = 1 - (1 - DE_{Bi})\left(1 - DE_{B(i+1)}\right) \ldots \left(1 - DE_{Bj}\right) \quad (3).$$

Then, the regional DF was calculated as

$$DF_{region} = DE_{region} * FR_{Bi} \quad (4)$$

where FR_{Bi} is the fraction remaining of drug entering the *i*th bifurcation. These calculations were performed for each SIP model and the DF values were then summed to provide total regional DF values. As with the branch-averaged DE calculations, the values of FR_{B4} for the LL, LU, and RU SIP models were applied using the summed amounts of mass from both B3 outlets of those lobes. DF and DE values were multiplied by 100 and expressed as percentages in the results based on typical convention.

Predictions of DF in the alveolar region were obtained for each of the four cases using the correlations developed by Khajeh-Hosseini-Dalasm and Longest.[36] A series of transient simulations were used to predict DF values for particles in the range of 0.5-10 μm injected into acinar models with 2, 3, and 4 generations that feature 14-hedron alveolar elements.[36] Dynamic meshing was used by Khajeh-Hosseini-Dalasm and Longest[36] to simulate wall motion through a uniform volume expansion and the transient waveforms tested were the

SD and QD profiles described earlier in this section and developed by Longest et al.[30] The results were used to develop correlations for deposition efficiency during SD inhalation, QD inhalation, and any subsequent breath-hold (BE), which were (expressed as a percentage)

$$DE_{SD}=\begin{cases} 100\left(1-0.96e^{-0.053\left(t_{res}{d_{ae}}^2\right)^{1.73}}\right), & 0<t_{res}<\frac{T}{2} \\ 100\left(1-0.83e^{-0.015\left({t_{res}}^2 d_{ae}\right)^{1.67}}\right), & \frac{T}{2}<t_{res}<T \end{cases} \quad (5a,b),$$

$$DE_{QD}=\begin{cases} 100\left(1-0.96e^{-0.017\left(t_{res}{d_{ae}}^2\right)^{2.17}}\right), & 0<t_{res}<\frac{T}{2} \\ 100\left(1-0.8e^{-0.093\left({t_{res}}^2 d_{ae}\right)^{1.7}}\right), & \frac{T}{2}<t_{res}<T \end{cases} \quad (6a,b),$$

and

$$DE_{BH}=100\left(1-e^{-0.0855\left(t_{res}{d_{ae}}^2\right)^{1.5}}\right) \quad (7),$$

where d_{ae} is the aerodynamic diameter of the aerosol, t_{res} is the potential maximum residence time in the acinar model, and T is the total period of inhalation. The value of t_{res} is found by subtracting the time of particle entrance into the alveolar region from T. For the case of the breath-hold, t_{res} is the prescribed breath-hold time. In this study, the breath-hold period was 10 s, which was the longest duration simulated by Khajeh-Hosseini-Dalasm and Longest,[36] and is frequently prescribed with correct inhaler usage.

Results

Mouth-throat and upper TB deposition

In the upper TB simulations, the constricted MDI and DPI models show approximately twice as much drug deposition as compared with their non-constricted counterparts, where the DF values in the upper TB region (i.e., DF_{TB}) increase from 1.2% to 2.7% with the MDI and from 2.9% to 5.7% with the DPI, as illustrated in Figure 3. Increased particle inertia as a result of accelerated velocities together with increased turbulent dispersion are responsible for this increase in deposition associated with constricted airways. Additionally, the extrathoracic regions for both the MDI and DPI models show a small increase in DF from the non-constricted to the constricted versions, where the total DF in the combination of the MP and MT regions in the MDI models increases from 51.1% to 53.4%, while the DF in the combination of the MP and MT regions of the of DPI models increases from 71.3% to 75.3%. This may be partly explained by the decrease in diameter from the glottis to the tracheal entrance, which comprises a small section of the MT region in both the MDI and DPI models. However, upstream effects of the increased pressure drop in the constricted model also appear to have an effect. In the MDI case, the MP deposition fraction increases from 5.4% to 9.1% while the MT region shows a slight decrease from 45.7% to 44.3%. With the DPI, the upstream effects appear to be confined to the MT region, which shows an increase in DF of 69.7% to 73.8% from the non-constricted to the constricted case, while the deposition in the MP region remains relatively constant. Compressible flow in the MDI case

used to capture the supersonic gas flow near the MDI nozzle[30] may enhance these upstream effects in the MP region as compared with the incompressible flow in the DPI case.

Aerosol mass distribution entering the lung lobes

Based on transport from the inhalers through the upper TB model, the normalized mass distribution of aerosols entering each of the lung lobes is presented in Table 2. The mass distributions are reported as the aerosol mass entering each of the lung lobes normalized by the average mass entering all five lobes. In all cases except for the MDI constricted case, the LL lobe receives approximately 30% more aerosol than the mean lobar values. Surprisingly, the combination of airway constriction and the large inertial burst[30,68] associated with firing the MDI shifts the maximum mass fraction to the RU lobe. In all cases, the RM lobe is shown to receive the least (~0.36-0.34) normalized mass of drug.

TB aerosol deposition

Particle deposition is illustrated with the LL SIP models in the middle TB (B4-B7) and lower TB (B8-B15) sections for all cases in Figures 4 and 5, since that lobe is most likely to be representative of average lobar values based on previous findings.[29] Deposition efficiency (DE) values in the middle TB sections (Figure 4) show generally decreasing DE values from B4 to B7, though a small rise in DE is observed from B5 to B6 for both MDI cases, and the DE values for the DPI non-constricted case are nearly constant. As expected for impaction, deposition location is typically centered on the carina of each bifurcation, but in the B4 and B5 regions particle deposition is also observed along the straight portions of the airways due to bifurcation rotation and multiple bifurcation flow effects.

The DE values in the lower TB sections (Figure 5) show an overall decrease from B8 to B12 or B13, but there is a significant increase from that point until B15 for all cases, except the MDI non-constricted case where DE is reduced from B14 to B15. As with the middle TB sections, there is an initial rise in DE values from B8 to B9, followed by a decreasing pattern. Similar to the pattern in the middle TB sections, the location of particle deposition is centered on the carina for all bifurcations, while deposition is also observed on the straight sections of B8 and B9.

Regional DF values for the predictions from the SIP models are given in Table 3. For both inhaler types, the amount of drug deposited in the lower TB (B8-B15) region decreases from the non-constricted cases to the constricted cases, with a reduction from 1.13% to 0.89% for MDI delivery and from 1.08% to 0.81% for DPI delivery. Considering the middle TB region, the DPI cases show a decrease from 1.85% in the non-constricted model to 1.38% in the constricted model, while for the MDI cases an increase is observed from 0.73% to 1.40%. This is most likely explained by the rise in DE values in the middle TB regions from the MDI non constricted case to the MDI constricted case, while a similar rise was not observed for the DPI cases. Similar to the middle TB region, DF values in the combined middle and lower TB region (B4-B15) show an increase from the MDI non-constricted case to the MDI constricted case of 1.86% to 2.29%, while from the DPI non-constricted case to the DPI constricted case a reduction of 2.93% to 2.19% is observed.

Comparison of regional deposition fractions

The DF predictions from the transient upper airway and steady state SIP simulations are given in Figure 6 along with the alveolar DF values obtained from the Khajeh-Hosseini-Dalasm and Longest[36] correlations. The MP and MT predictions are combined to provide an indication of total drug losses prior to tracheobronchial entry. Upper and middle TB deposition, which is defined here as the total DF from B1 to B7, is 1.9% and 4.1% for the MDI non-constricted and constricted cases, respectively, and 6.1% and 7.1% for the DPI non-constricted and constricted predictions. These values, which are an order of magnitude less than the loss in the MP and MT regions, indicate that the DPI may provide more efficient delivery to the upper lung airways than the MDI. Constriction in the upper lung airways shows relative increases of 116% and 16% in the DF values for the MDI and DPI cases, respectively, suggesting that while constriction is an important consideration for both delivery modes, it may be more important for characterizing MDI aerosol delivery. As discussed above, the lower TB (B8-B15) values of DF in the MDI and DPI non-constricted cases are both about 1%, with an absolute decrease in DF values of about 0.2% for both the constricted cases as compared with the non-constricted results.

Alveolar DF predictions show opposite trends as compared to those observed in the upper airways. Alveolar deposition in the MDI non-constricted and constricted cases is higher than for the DPI cases, with DF values of 41.4% and 37.5% for both MDI cases, respectively, and for the DPI cases the values are 20.7% and 14.1%. With less drug lost in the MP and MT regions for the MDI cases, there is significantly more drug available for alveolar deposition than for the DPI cases. Also, constricted DF values in the alveolar region are reduced for both the MDI and DPI, presumably because in the constricted models more drug deposits in the extrathoracic and upper airway regions as compared with the non-constricted models, leaving less available for deposition in the alveolar region.

Deposition in the small TB airways (< 2 mm diameter)

To better understand the distribution of drug deposition in the small airways, the values of DF are divided between the large TB airway (> 2 mm diameter) and the small TB airway (< 2 mm diameter) sub-regions and illustrated in Figure 7. The results show an even greater difference between large and small TB airway DF values as compared with the corresponding difference between DF in the B1-B7 and B8-B15 airways. For the MDI delivery cases, the DF values in the large and small TB airways in the healthy model are 2.7% versus 0.4%, and for the asthmatic model the respective values are 4.3% and 0.3%. The DF results for DPI delivery were 5.4% and 0.4% in the large and small TB airways of the healthy model, respectively, while the corresponding predictions for the asthmatic model were 7.6% and 0.3%. Altogether, the DF predictions in the small TB airways were on the order of 0.3-0.4%.

Discussion

A primary finding of this study is that the small TB airways, which are typically inflamed in asthma[2,7,8,21,22] and contain the important terminal bronchioles, receive very little medication (~1% of the aerosolized dose) with conventional MDI and DPI aerosols. This

study provides first estimates of pharmaceutical aerosol deposition in the lower TB region (B8-B15) of an asthmatic airway model, where both MDI and DPI aerosols were considered. The DF predictions show relatively small amounts of drug delivered to the lower TB airways, which was ~1% of the aerosolized dose for all cases. By comparison, the mass of drug delivered to the combination of the upper and middle TB regions was two to seven times greater than to the lower TB airways. Drug delivery to the lower TB airways of the constricted models was slightly less than with the healthy models. The net reductions in DF values in the lower TB airways for both MDI and DPI delivery from the non-constricted to the constricted models were 0.24% and 0.27%, respectively, which represent significant decreases on a relative basis (21% and 25%), though biological dose-response testing is needed to quantify the impact of these predicted differences. As an additional point of comparison, values of DF in the small TB airways (< 2 mm diameter) as defined in the literature[1,16-18] were estimated to be even lower than for the lower TB region, with about 0.3-0.4% of the aerosolized dose for all cases.

The effect of the small amount of predicted drug delivery to the lower TB airways would be further amplified by the exponential increase in surface area as a function of depth into the lungs. As mentioned in the Introduction, regional lung surface areas may be estimated using the measurements of Yeh and Schum[19] as 0.2 m^2 in the lower TB airways as compared with 0.1 m^2 in the combination of the upper and middle airways.

To visualize the distribution of particles in different regions of the lung in terms of dose per unit surface area, 1 cm^2 representative samples of lung tissue are displayed in Figure 8. For this visualization, it was assumed that a 250 μg dose of fluticasone propionate was initially aerosolized and had a monodisperse particle size of 2.64 μm resulting in 19,808,806 initial particles. Based on the predicted DF in each region for the MDI in the non-constricted airway and the regional lung surface areas, the number of particles that would deposit in a 1 cm^2 area of each lung region is illustrated in Figure 8. The deposition locations are distributed randomly within the 1 cm^2 areas only for illustration and the size of the particle markers are not to scale. This visualization represents how sparse deposition becomes in the lower TB and alveolar regions. Viewed another way, the drug dose that would be delivered to each 1 cm^2 tissue section is also represented in Figure 8 for the case of the MDI and non-constricted airways. While the MT tissue sample (1 cm^2) would receive 0.71 μg of drug, the lower TB and alveolar regions would only receive 1.25 and 0.17 ng, respectively. Although fluticasone propionate is a potent molecule, it is difficult to envision that a 0.17 ng dose per cm^2 would be therapeutically effective in the alveolar region.

Assuming an aerosolized dose of 250 μg from both inhalers and the previously specified lung surface areas, total dose per unit-surface-area in each lung region is reported in Figure 9. Only the MT deposition is considered for the extrathoracic region, as opposed to Figure 6 where both the MP and MT deposition values are considered together. Within each region the same trends (increasing vs. decreasing) between cases are observed as in Figure 6, except for the MT region which is slightly different since the MP deposition was omitted. Considering all four cases, the values of dose per unit-surface-area in the lower TB region range from 9.0×10^{-4} to 1.3×10^{-3} μg/cm^2, which represent a four- to twenty-fold decrease when compared with the results from the combined upper and middle TB region. Alveolar

dose per unit-surface-area is even less than for the lower TB region, ranging from 5.6×10^{-5} to 1.7×10^{-4} μg/cm^2. Across the lung, dose per unit-surface-area varies by approximately two orders of magnitude. When the MT region is included, dose per unit-surface-area varies by four orders of magnitude. Altogether, it is clear that the CFD predictions show that uniform dosing on a regional basis is not achieved with the inhalers considered upon initial particle deposition.

Based on one-dimensional (1D) whole-lung model predictions and monodisperse bolus *in vivo* inhalation experiments, aerodynamic particle sizes of approximately 3 μm and below are typically viewed as effectively penetrating the upper TB region and reaching the small airways.[32-34] However, results of this study demonstrate low deposition in the small TB airways for both inhalers and a relatively low alveolar deposition fraction for the DPI, even at initial MMADs less than 3 μm. This ineffective small airway delivery is due to high upper airway depositional losses stemming from turbulence and aerodynamic factors associated with the DPI and MDI inhalers.[30] Increasing small airway deposition may require even smaller particle sizes; however, particle sizes below approximately 1.5 μm are expected to result in exhalation of the aerosol before deposition can occur,[32] depending on the period of breath hold. Clinically, reduced particle sizes for inhaled corticosteroids generated from MDIs have demonstrated improved asthma treatment.[1,26,73] A potential concern with reduced size is increased alveolar deposition leading to systemic absorption of the medication and associated corticosteroid side effects such as adrenal suppression. In contrast with this concern, it is observed that inflammation associated with asthma occurs at all levels of the lung making small airway delivery therapeutically effective.[1,2] Surprisingly, Harrison[74] observed that particle size reduction associated with switching from CFC to HFA MDIs did not increase systemic exposure to beclomethasone dipropionate (BDP), but instead reduced systemic exposure due to reduced MT deposition. Harrison[74] points out that the additional alveolar dose of BDP is likely clinically beneficial, similar to expectations from more recent reviews.[1,73,75] Still, pharmaceutical scientists and clinicians should remain aware of the potential for increased systemic drug exposure associated with increasing small airway delivery intended to treat asthmatic inflammation throughout the lungs.

The lower TB airway DF predictions obtained for this study agree well with those from a recent study by Longest et al.,[29] who used SIP models to predict lower TB airway DF in a healthy lung model with DPI delivered albuterol sulfate. Comparison of the DPI non-constricted DF value in the lower TB airway region with the results of Longest et al.[29] indicates 1.08% for the Flovent Diskus DPI in this study as opposed to 0.9% with the Novolizer DPI.[29] Although inhaled pharmaceutical aerosols are nearly always polydisperse in nature, a direct comparison of the polydisperse data from this study with other published studies was difficult to obtain. Previously, CFD investigations into DF or DE values between non-constricted and constricted airways were conducted by simulating multiple cases with monodisperse particle injections over a certain range as a means of capturing the filtering capacity of the airways of interest for use in 1D whole-lung models.[40,42,45] Moreover, the previous asthma CFD models often focused on only a few bifurcations, as opposed to the complete CFD lung model considered here.[42,45] Vinchurkar et al.[41] evaluated aerosol delivery in five patient-specific models of asthmatics that extended as far

as the ninth bifurcation level using CFD to predict MDI delivery of beclomethasone propionate/formoterol at 15, 30, and 60 L/min. Thoracic deposition was estimated by Vinchurkar et al.[41] to be 28.3 ± 8.3%, 26.3 ± 8.6%, and 22.9 ± 8.6% when the aerosol was released between 0 and 0.3 s for the three flow rates, respectively, which were all lower than the DF of 42.5% reported for MDI delivery to the constricted model in this study. The smaller deposited mass reported by Vinchurkar et al.[41] may be explained by the smaller mass median aerodynamic diameter (MMAD) of the formulation used in that study (1.30 μm) as compared with the MDI particle distribution used in the current simulations (2.64 μm). Additional differences between these two studies include the assumption by Vinchurkar et al.[41] that particles penetrating beyond the upper TB airways deposit in the lungs and the use of patient specific vs. characteristic airway models.

As described in the Introduction, the whole-lung CFD-based modeling approach employed in this study accurately predicted (within 10% relative error) regional *in vivo* lung deposition data for a characteristic DPI and the Respimat spray inhaler.[72] These model and *in vivo* comparisons were limited to the 2D projected lung regions identified in the *in vivo* data.[72] In the future, model validations are needed based on comparisons with recent 3D *in vivo* aerosol deposition data. For example, Fleming et al.[76] report 3D *in vivo* lung deposition data for aerosols from two different nebulizers based on a nested shell representation of the lung, which is mapped to different lung generation levels. Conway et al.[77] report both 2D and 3D lung deposition *in vivo* data for well controlled particle sizes and inspiratory patterns together with patient-specific airway anatomy for a nebulized aerosol. Comparison of the Conway et al.[77] data with a 1D lung deposition model showed limited agreement highlighting the need to improve lung deposition estimates, even for nebulized aerosols. An advantage of the Tian et al.[72] *in vivo* validation study of CFD model predictions is the consideration of airway deposition data using a DPI and the Respimat spray inhaler, which are known to modify airway deposition patterns compared with nebulized aerosols that are slowly inhaled. The Tian et al.[72] validation study did not compare MDI deposition predictions with *in vivo* data. Instead, previous studies and the current study validated model predictions for the MDI with concurrent *in vitro* data in a characteristic MT geometry,[30] where the MT geometry was shown to match *in vivo* aerosol deposition for a range of DPI aerosols.[78,79] Future studies are needed to further validate MDI predictions with *in vivo* data across a range of relevant particle sizes produced by commercial products.

Among the limitations of the study was the assumption that five SIP geometries would provide an adequate representation of branch-averaged DE based on the study of Longest et al.,[30] but it is possible that the addition of more SIP geometries may affect the data. The constricted models were constructed assuming a 30% diameter reduction in order to capture homogenous long-term airway remodeling associated with inflammation,[7,59] but not an acute asthma attack. The combination of transient and steady simulations with interpolation of fluid velocities and particle trajectories is an assumption based on the findings of Tian et al.,[31] but full transient simulations may further improve accuracy. Lastly, for computational efficiency turbulence was modeled using a Reynolds-averaged Navier-Stokes (RANS) approximation, but a model that captures more of the eddy characteristics, such as a large eddy model, would provide a more complete physical representation of the deposition

mechanisms,[80,81] though it would present significant challenges in terms of the computational time required to simulate a full transient inspiratory breath.

Conclusions

Regional DF and branch-averaged DE values were predicted using CFD methods in conjunction with improved near-wall corrections of particle trajectories for MDI and DPI delivery through non-constricted and inflammation constricted lung models from the MT through B15. The branch-averaged DE predictions obtained from the CFD data were used to provide the first known CFD estimates of DF in the lower TB airways (B8-B15) for an asthmatic subject, where it was shown that values in the MDI and DPI non-constricted cases were 1.13% and 1.08%, respectively, which were reduced to constricted model values of 0.89% and 0.81%. Predictions for the combined upper and middle TB (B1-B7) DF values were two- to seven-fold higher than the lower TB region. When the DF values were adjusted to consider small TB airway (< 2 mm diameter) deposition, the DF values dropped to a range of 0.3-0.4% for all cases. The deposited dose per unit-surface-area results were 9.0×10^{-4} to 1.3×10^{-3} μg/cm^2 in the lower TB region, which represented a four- to twenty-fold decrease from the combined upper and middle TB region predictions and indicated that uniform dosing on a regional basis does not occur for each of the four cases considered. Area normalized deposition in the alveolar region was even lower, ranging from 5.6×10^{-5} to 1.7×10^{-4} μg/cm^2. The deposition fraction and the dose per unit-surface-area predictions in the lower TB and alveolar airways suggest that inefficient delivery of medications to those regions may be a significant component of uncontrolled asthma.

Acknowledgments

Helpful conversations with Dr. Michael Hindle (VCU Department of Pharmaceutics) are gratefully acknowledged. This study was supported by Award U01 FD004570 from the US FDA and Award R01 HL107333 from the National Heart, Lung, and Blood Institute. The content is solely the responsibility of the authors and does not necessarily represent the official views of the US FDA, the National Heart, Lung, and Blood Institute or the National Institutes of Health.

Abbreviations

1D	one-dimensional
B*i*	*i*th bifurcation (trachea and main bronchi are B1)
CFC	chlorofluorocarbon
CFD	computational fluid dynamics
COPD	chronic obstructive pulmonary disease
CT	computed tomography
DE	deposition efficiency
DF	deposition fraction
DPI	dry powder inhaler
d_{ae}	aerodynamic particle diameter

FEF	forced expiratory flow
FEV_1	forced expiratory volume in 1 s
FR_{Bi}	fraction remaining of drug entering the *i*th bifurcation
FRC	functional residual capacity
G*i*	airway generation number (trachea is G0)
GSD	geometric standard deviation
HFA	hydrofluoroalkane
k	turbulent kinetic energy
LU	left upper
LL	left lower
LRN	low Reynolds number
MDI	metered dose inhaler
MMAD	mass median aerodynamic diameter
MP	mouthpiece
MT	mouth-throat
n	wall-normal coordinate
n^+_{limit}	upper limit for application of anisotropic fluctuating velocity correction
nw_{limit}	near-wall limit
PET	positron emission tomography
PIFR	peak inspiratory flow rate
PRB	physically realistic bifurcation
QD	quick and deep
RANS	Reynolds averaged Navier-Stokes
RL	right lower
RM	right middle
RU	right upper
SD	slow and deep
SIP	stochastic individual path
T	period of inhalation
TB	tracheobronchial
t_{res}	potential maximum residence time
UDF	user defined function

y^+	wall y-plus value
ω	specific rate of turbulence dissipation

References

1. Usmani OS, Barnes PJ. Assessing and treating small airways disease in asthma and chronic obstructive pulmonary disease. Ann Med. 2012; 44:146–156. [PubMed: 21679101]
2. Hamid Q, Song Y, Kotsimbos TC, Minshall E, Bai TR, Hegele RG, Hogg JC. Inflammation of small airways in asthma. J Allergy Clin Immunol. 1997; 100:44–51. [PubMed: 9257786]
3. Hogg JC, Macklem PT, Thurlbeck WM. Site and nature of airway obstruction in chronic obstructive lung disease. N Engl J Med. 1968; 278:1355–1360. [PubMed: 5650164]
4. Bennett WD, Smaldone GC. Use of aerosols to estimate mean air-space in chronic obstructive pulmonary disease. J Appl Physiol. 1988; 64(4):1554–1560. [PubMed: 3378990]
5. Carroll N, Elliot J, Morton A, James A. The structure of large and small airways in nonfatal and fatal asthma. Am Rev Respir Dis. 1993; 147:405–410. [PubMed: 8430966]
6. Yanai M, Sekizawa K, Ohrui T, Sasaki H, Takishima T. Site of airway obstruction in pulmonary disease: direct measurement of intrabronchial pressure. J Appl Physiol. 1992; 72(3):1016–1023. [PubMed: 1568955]
7. Kuwano K, Bosken CH, Paré PD, Bai TR, Wiggs BR, Hogg JC. Small airways dimensions in asthma and in chronic obstructive pulmonary disease. Am Rev Respir Dis. 1993; 148:1220–1225. [PubMed: 8239157]
8. Wiggs BR, Bosken C, Paré PD, James A, Hogg JC. A model of airway narrowing in asthma and in chronic obstructive pulmonary disease. Am Rev Respir Dis. 1992; 145:251–258. [PubMed: 1736725]
9. Gelfrand EW, Kraft M. The importance and features of the distal airways in children and adults. J Allergy Clin Immunol. 2009; 124:S84–S87. [PubMed: 19962041]
10. Barnes PJ. Severe asthma: advances in current management and future therapy. J Allergy Clin Immunol. 2012; 129:48–59. [PubMed: 22196524]
11. Chapman KR, Boulet LP, Rea RM, Franssen E. Suboptimal asthma control: prevalence, detection and consequences in general practice. Eur Respir J. 2008; 31:320–325. [PubMed: 17959642]
12. Partridge MR, van der Molen T, Myrseth S-E, Busse WW. Attitudes and actions of asthma patients on regular maintenance therapy: the INSPIRE study. BioMed Central Pulmonary Medicine. 2006; 6:13. [PubMed: 16772035]
13. Biddiscombe MF, Usmani OS, Barnes PJ. A system for the production and delivery of monodisperse salbutamol aerosols to the lungs. Int J Pharm. 2003; 254:243–253. [PubMed: 12623200]
14. Usmani OS, Biddiscombe MF, Nightingale JA, Underwood SR, Barnes PJ. Effects of bronchodilator particle size in asthmatic patients using monodisperse aerosols. J Appl Physiol. 2003; 95:2106–2112. [PubMed: 12897033]
15. Usmani OS, Biddiscombe MF, Barnes PJ. Regional lung deposition and bronchodilator response as a function of β2-agonist particle size. Am J Respir Crit Care Med. 2005; 172:1497–1504. [PubMed: 16192448]
16. Weibel, ER. Morphometry of the Human Lung. Springer Verlag; Berlin: 1963.
17. Mead J. The lung's "quiet zone". N Engl J Med. 1970; 282:1318–1319. [PubMed: 5442364]
18. Baraldo S, Saetta M, Cosio MG. Pathophysiology of the small airways. Semin Respir Crit Care Med. 2003; 24(5):465–472. [PubMed: 16088567]
19. Yeh HC, Schum GM. Models of human lung airways and their application to inhaled particle deposition. Bull Math Biology. 1980; 42:461–480.
20. ICRP. Human Respiratory Tract Model for Radiological Protection. Elsevier Science Ltd; New York: 1994.

21. Kraft M, Martin RJ, Wilson S, Djukanovic R, Holgate ST. Lymphocyte and eosinophil influx into alveolar tissue in nocturnal asthma. Am J Respir Crit Care Med. 1999; 150:228–234. [PubMed: 9872843]
22. Kraft M, Djukanovic R, Wilson S, Holgate ST, Martin RJ. Alveolar tissue inflammation in asthma. Am J Respir Crit Care Med. 1996; 154(5):1505–1510. [PubMed: 8912772]
23. Gentile DA, Skoner DP. New asthma drugs: small molecule inhaled corticosteroids. Curr Opin Pharmacol. 2010; 10:260–265. [PubMed: 20561819]
24. Fardon TC, Burns P, Barnes ML, Lipworth BJ. A comparison of 2 extrafine hydrofluoroalkane-134a-beclomethasone formulations on methacholine hyperresponsiveness. Ann Allergy Asthma Immunol. 2009; 96:422–430. [PubMed: 16597076]
25. Cohen J, Douma WR, ten Hacken NHT, Vonk JM, Oudkerk M, Postma DS. Ciclesonide improves measures of small airway involvement in asthma. Eur Respir J. 2008; 31:1213–1220. [PubMed: 18287130]
26. Bulac S, Cimrin A, Elidokuz H. The effect of beclometasone dipropionate/formoterol extra-fine fixed combination on the peripheral airway inflammation in controlled asthma. Journal of Aerosol Medicine and Pulmonary Drug Delivery. 2015; 28:82–87. [PubMed: 25050594]
27. Dhillon S, Keating GM. Beclometasone Dipropionate/Formoterol: In an HFA-propelled pressurised metered-dose inhaler. Drugs. 2006; 66(11):1475–1483. [PubMed: 16906779]
28. Kim KT, Milgrom H, Yoon K, Levy AL, Matz P, Welch MJ, Cahn A, Collins DA, Kathman S, Mehta R, Su S-F, Kunka RL. Systemic exposure and urinary cortisol effects of fluticasone propionate formulated with hydrofluoroalkane in 4-11-year-olds with asthma. J Clin Pharmacol. 2008; 48:108–116. [PubMed: 18094223]
29. Longest PW, Tian G, Delvadia R, Hindle M. Development of a stochastic individual path (SIP) model for predicting the deposition of pharmaceutical aerosols: Effects of turbulence, polydisperse aerosol size, and evaluation of multiple lung lobes. Aerosol Science and Technology. 2012; 46(12):1271–1285.
30. Longest PW, Tian G, Walenga RL, Hindle M. Comparing MDI and DPI aerosol deposition using in vitro experiments and a new stochastic individual path (SIP) model of the conducting airways. Pharm Res. 2012; 29:1670–1688. [PubMed: 22290350]
31. Tian G, Longest PW, Su G, Walenga RL, Hindle M. Development of a stochastic individual path (SIP) model for predicting the tracheobronchial deposition of pharmaceutical aerosols: Effects of transient inhalation and sampling the airways. J Aerosol Sci. 2011; 42:781–799.
32. Kim CS. Deposition of aerosol particles in human lungs: in vivo measurement and modelling. Biomarkers. 2009; 14(sup1):54–58. [PubMed: 19604060]
33. Martonen T, Fleming J, Schroeter J, Conway J, Hwang D. In silico modeling of asthma. Advanced Drug Delivery Reviews. 2003; 55:829–849. [PubMed: 12842603]
34. Martonen TB, Musante CJ, Segal RA, Schroeter JD, Hwang D, Dolovich MA, Burton R, Spencer RM, Fleming JS. Lung models: strengths and limitations. Respiratory Care. 2000; 45(6):712–736. [PubMed: 10894463]
35. Tian G, Longest PW, Su G, Hindle M. Characterization of respiratory drug delivery with enhanced condensational growth (ECG) using an individual path model of the entire tracheobronchial airways. Ann Biomed Eng. 2011; 39(3):1136–1153. [PubMed: 21152983]
36. Khajeh-Hosseini-Dalasm N, Longest PW. Deposition of particles in the alveolar airways: inhalation and breath-hold with pharmaceutical aerosols. J Aerosol Sci. 2015; 79:15–30. [PubMed: 25382867]
37. Chan TL, Lippmann M. Experimental measurement and empirical modeling of the regional deposition of inhaled particles in humans. Am Ind Hyg Assoc J. 1980; 41:399–409. [PubMed: 7395753]
38. Stahlhofen W, Rudolf G, James AC. Intercomparison of experimental regional aerosol deposition data. J Aerosol Med. 1989; 2(3):285–308.
39. Scheuch G, Bennett W, Borgström L, Clark A, Dalby R, Dolovich M, Fleming J, Gehr P, Gonda I, O'Callaghan C, Taylor G, Newman S. Deposition, Imaging, and Clearance: What Remains to be Done? J Aerosol Med Pulm Drug Deliv. 2010; 23:S39–S57. [PubMed: 21133799]

40. Inthavong K, Tu J, Ye Y, Ding S, Subic A, Thien F. Effects of airway obstruction induced by asthma attack on particle deposition. J Aerosol Sci. 2010; 41:587–601.
41. Vinchurkar S, De Backer L, Vos WG, Van Holsbeke C, De Backer J, De Backer W. A case series on lung deposition analysis of inhaled medication using functional imaging based computational fluid dynamics in asthmatic patients: effect of upper airway morphology and comparision with in vivo data. Inhal Toxicol. 2012; 24(2):81–88. [PubMed: 22260527]
42. Longest PW, Vinchurkar S, Martonen TB. Transport and deposition of respiratory aerosols in models of childhood asthma. J Aerosol Sci. 2006; 37:1234–1257.
43. Zhang H, Papadakis G. Computational analysis of flow structure and particle deposition in a single asthmatic human airway bifurcation. J Biomech. 2010; 43:2453–2459. [PubMed: 20646710]
44. Yang XL, Liu Y, Luo HY. Respiratory flow in obstructed airways. J Biomech. 2006; 39:2743–2751. [PubMed: 16300771]
45. Farkas A, Balashazy I. Simulation of the effect of local obstructions and blockage on airflow and aerosol deposition in central human airways. J Aerosol Sci. 2007; 38:865–884.
46. Tgavalekos NT, Tawhai M, Harris RS, Mush G, Vidal-Melo M, Venegas JG, Lutchen KR. Identifying airways responsible for heterogeneous ventilation and mechanical dysfunction in asthma: an image functional modeling approach. J Appl Physiol. 2005; 99(6):2388–2397. [PubMed: 16081622]
47. Raabe OG, Yeh HC, Schum GM, Phalen RF. Tracheobronchial geometry: human, dog, rat, hamster. 1976 Report No LF-53.
48. Parker H, Horsfield K, Cumming G. Morphology of distal airways in the human lung. J Appl Physiol. 1971; 31:386–391. [PubMed: 4939280]
49. Koblinger L, Hofmann W. Analysis of human lung morphometric data for stochastic aerosol deposition calculations. Phys Med Biol. 1985; 30(6):541–556. [PubMed: 4011676]
50. Horsfield K, Dart G, Olson DE, Filley GF, Cumming G. Models of the human bronchial tree. J Appl Physiol. 1971; 31:207–217. [PubMed: 5558242]
51. Xi, J.; Longest, PW. Effects of improved near-wall modeling on micro-particle deposition in oral airway geometries. Proceedings of the 2007 ASME Summer Bioengineering Conference, Keystone, CO Paper No. SBC2007-176227; 2007.
52. Walenga RL, Tian G, Longest PW. Development of characteristic upper tracheobronchial airway models for testing pharmaceutical aerosol delivery. J Biomech Eng. 2013; 135:091010.
53. Heistracher T, Hofmann W. Physiologically realistic models of bronchial airway bifurcations. J Aerosol Sci. 1995; 26(3):497–509.
54. Hammersley JR, Olson DE. Physical models of the smaller pulmonary airways. J Appl Physiol. 1992; 72:2402–2414. [PubMed: 1629097]
55. Russo J, Robinson R, Oldham MJ. Effects of cartilage rings on airflow and particle deposition in the trachea and main bronchi. Med Eng Phys. 2008; 30:581–589. [PubMed: 17719260]
56. Elias JA, Zhu Z, Chupp G, Homer RJ. Airway remodeling in asthma. Journal of Clinical Investigation. 1999; 104(8):1001. [PubMed: 10525034]
57. Vignola AM, Mirabella F, Costanzo G, Di Giorgi R, Gjomarkaj M, Bellia V, Bonsignore G. Airway remodeling in asthma. CHEST Journal. 2003; 123(3_suppl):417S–422S.
58. Ketai L, Coutsias C, Williamson S, Coutsias V. Thin-section CT evidence of bronchial thickening in children with stable asthma: bronchoconstriction or airway remodeling? Academic radiology. 2001; 8(3):257–264. [PubMed: 11249090]
59. Sumi Y, Hamid Q. Airway remodeling in asthma. Allergology International. 2007; 56(4):341–348. [PubMed: 17965577]
60. James AL. Relationship between airway wall thickness and airway hyperresponsiveness. Airway wall remodelling in asthma. 1997:1.
61. Walenga, RL. Mechanical and Nuclear Engineering. Virginia Commonwealth University; Richmond, VA: 2014. CFD assessment of respiratory drug delivery efficiency in adults and improvements using controlled condensational growth.

62. Broeders MEAC, Molema J, Hop WCJ, Folgering HTM. Inhalation profiles in asthmatics and COPD patients: Reproducibility and effect of instruction. J Aerosol Med. 2003; 16(2):131–141. [PubMed: 12823907]

63. Asgharian B, Price OT. Airflow distribution in the human lung and its influence on particle deposition. Inhal Toxicol. 2006; 18:795–801. [PubMed: 16774869]

64. Yin Y, Choi J, Hoffman EA, Tawhai MH, Lin C-L. Simulation of pulmonary air flow with a subject-specific boundary condition. J Biomech. 2010; 43:2159–2163. [PubMed: 20483412]

65. Longest PW, Hindle M, Das Choudhuri S, Byron PR. Numerical simulations of capillary aerosol generation: CFD model development and comparisons with experimental data. Aerosol Sci Tech. 2007; 41(10):952–973.

66. Longest PW, Xi J. Condensational growth may contribute to the enhanced deposition of cigarette smoke particles in the upper respiratory tract. Aerosol Sci Tech. 2008; 42:579–602.

67. Longest PW, Hindle M. Evaluation of the Respimat Soft Mist inhaler using a concurrent CFD and in vitro approach. J Aerosol Med Pulm Drug Deliv. 2009; 22(2):99–112. [PubMed: 18956950]

68. Longest, PW.; Hindle, M.; Das Choudhuri, S.; Byron, PR. Developing a better understanding of spray system design using a combination of CFD modeling and experiment. In: Dalby, RN.; Byron, PR.; Peart, J.; Suman, JD.; Farr, SJ.; Young, PM., editors. Proceedings of Respiratory Drug Delivery 2008. Davis Healthcare International Publishing; Illinois: 2008. p. 151-163.

69. Matida EA, Finlay WH, Grgic LB. Improved numerical simulation of aerosol deposition in an idealized mouth-throat. J Aerosol Sci. 2004; 35:1–19.

70. Longest PW, Xi J. Effectiveness of direct Lagrangian tracking models for simulating nanoparticle deposition in the upper airways. Aerosol Sci Tech. 2007; 41(4):380–397.

71. Matida EA, Nishino K, Torii K. Statistical simulation of particle deposition on the wall from turbulent dispersed pipe flow. International Journal of Heat and Fluid Flow. 2000; 21:389–402.

72. Tian G, Hindle M, Lee S, Longest PW. Validating CFD predictions of pharmaceutical aerosol deposition with *in vivo* data. Pharmaceutical Research. 2015 DOI 10.1007/s11095-015-1695-1.

73. Postma DS, van den Berge M. Small airway dysfunction in asthma and COPD: Consequences for therapy and the future. Respiratory Drug Delivery Europe. 2013; 2013:1–11.

74. Harrison LI. Local versus total systemic bioavailability of beclomethasone dipropionate CFC and HFA metered dose inhaler formulations. Journal of aerosol medicine. 2002; 15(4):401–406. [PubMed: 12581506]

75. Contoli M, Bousquet J, Fabbri LM, Magnussen H, Rabe KF, Siafakas NM, Hamid Q, Kraft M. The small airways and distal lung compartment in asthma and COPD: a time for reappraisal. Allergy. 2009; 65(2):141–151. [PubMed: 19909298]

76. Fleming JS, Epps BP, Conway JH, Martonen TB. Comparison of SPECT aerosol deposition data with a human respiratory tract model. Journal of aerosol medicine. 2006; 19(3):268–278. [PubMed: 17034303]

77. Conway J, Fleming J, Majoral C, Katz I, Perchet D, Peebles C, Tossici-Bolt L, Collier L, Caillibotte G, Pichelin M. Controlled, parametric, individualized, 2-D and 3-D imaging measurements of aerosol deposition in the respiratory tract of healthy human subjects for model validation. Journal of Aerosol Science. 2012; 52:1–17.

78. Delvadia R, Hindle M, Longest PW, Byron PR. In vitro tests for aerosol deposition II: IVIVCs for different dry powder inhalers in normal adults. Journal of aerosol medicine and pulmonary drug delivery. 2013; 26(3):138–144. [PubMed: 22947131]

79. Delvadia RR, Longest PW, Byron PR. In vitro tests for aerosol deposition. I: Scaling a physical model of the upper airways to predict drug deposition variation in normal humans. Journal of aerosol medicine and pulmonary drug delivery. 2012; 25(1):32–40. [PubMed: 22070526]

80. Jayaraju ST, Brouns M, Lacor C, Belkassem B, Verbanck S. Large eddy and detached eddy simulations of fluid flow and particle deposition in a human mouth-throat. Aerosol Science. 2008; 39:862–875.

81. Lambert AR, O'Shaughnessy PT, Tawhai MH, Hoffman EA, Lin C-L. Regional deposition of particles in an image-based airway model: Large-eddy simulation and left-right lung ventilation asymmetry. Aerosol Sci Tech. 2011; 45:11–25.

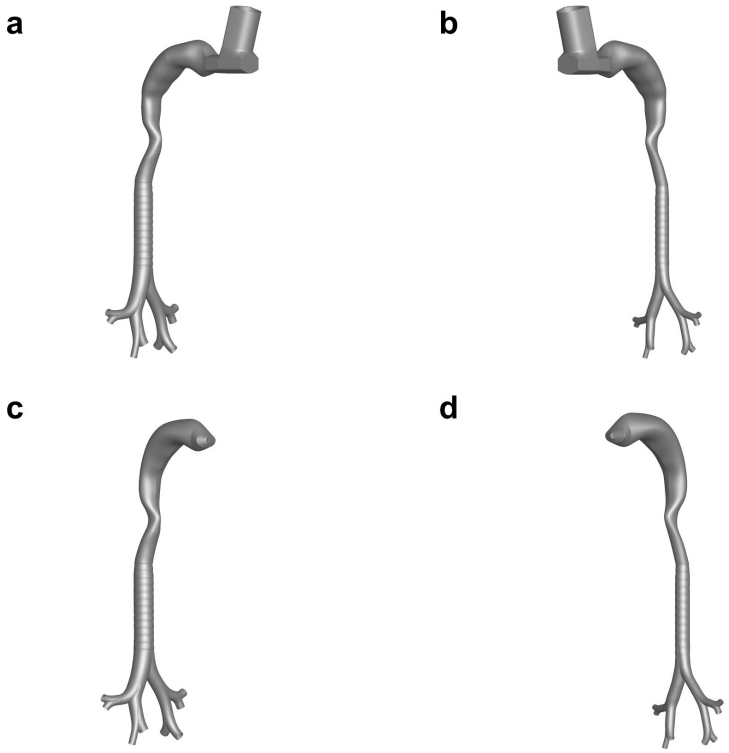

Figure 1.
Interior airspace of non-constricted and inflammation constricted mouth-throat (MT) plus upper tracheobronchial (TB) airways with a metered dose inhaler (MDI) (a and b) and with a dry powder inhaler (DPI) (c and d).

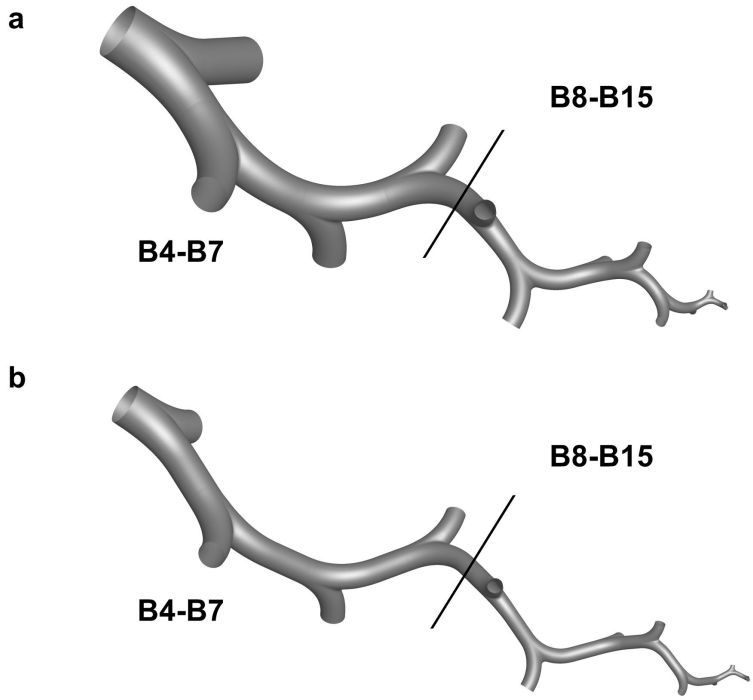

Figure 2.
Stochastic individual path (SIP) models of the left lower (LL) lobe from the fourth bifurcation (B4) through the fifteenth bifurcation (B15) for the (a) non-constricted and (b) inflammation constricted cases. The models are divided at the interface of B4-B7 and B8-B15 to illustrate the different lung regions of interest.

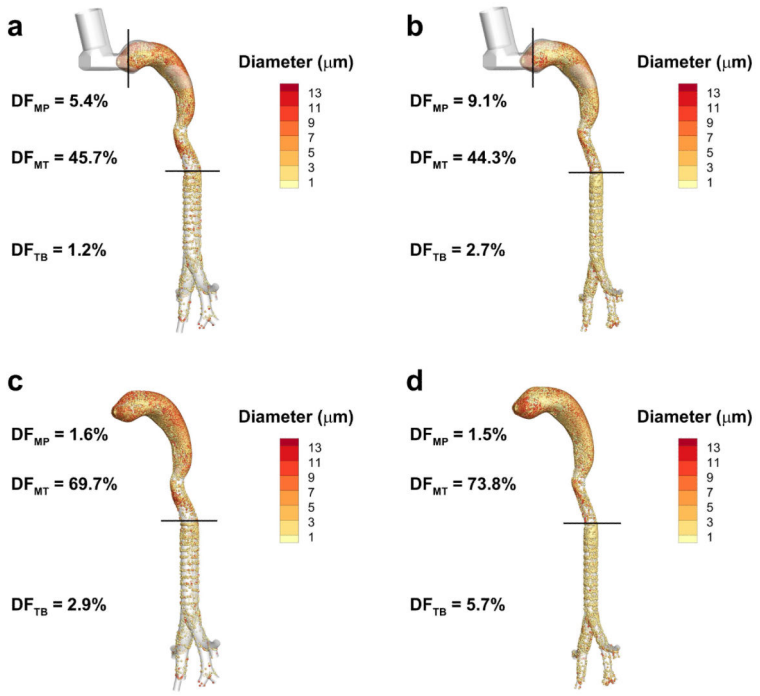

Figure 3.

Deposition fraction (DF) predictions (percentage of aerosolized drug mass) in the mouthpiece (MP), mouth-throat (MT) and upper tracheobronchial (TB) regions for the non-constricted and constricted airways with metered dose inhaler (MDI) delivery (a and b) and with dry powder inhaler (DPI) delivery (c and d).

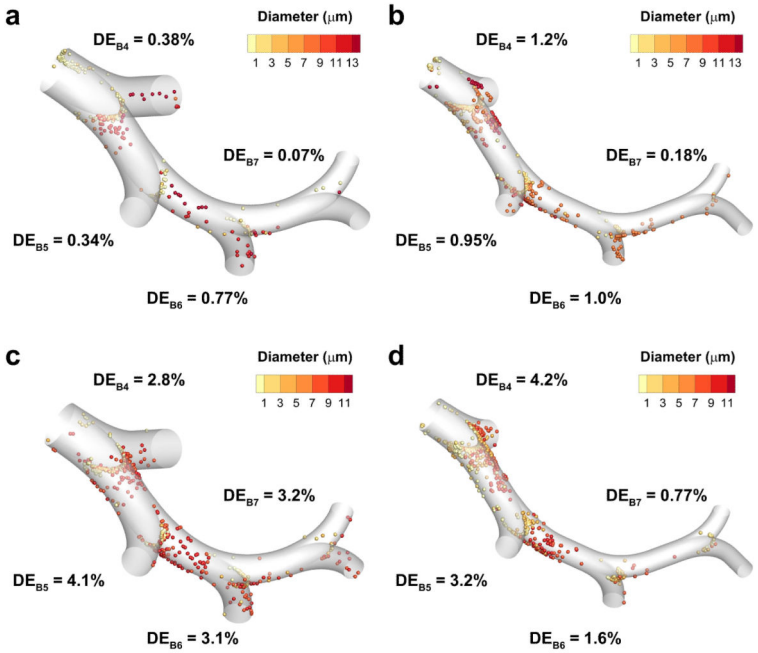

Figure 4.

Deposition efficiency (DE) estimates based on CFD predictions for the fourth through the seventh bifurcations (B4-B7) of the left lower (LL) lobe stochastic individual path (SIP) model. The cases presented are for non-constricted and constricted airways with metered dose inhaler (MDI) delivery (a and b) and with dry powder inhaler (DPI) delivery (c and d).

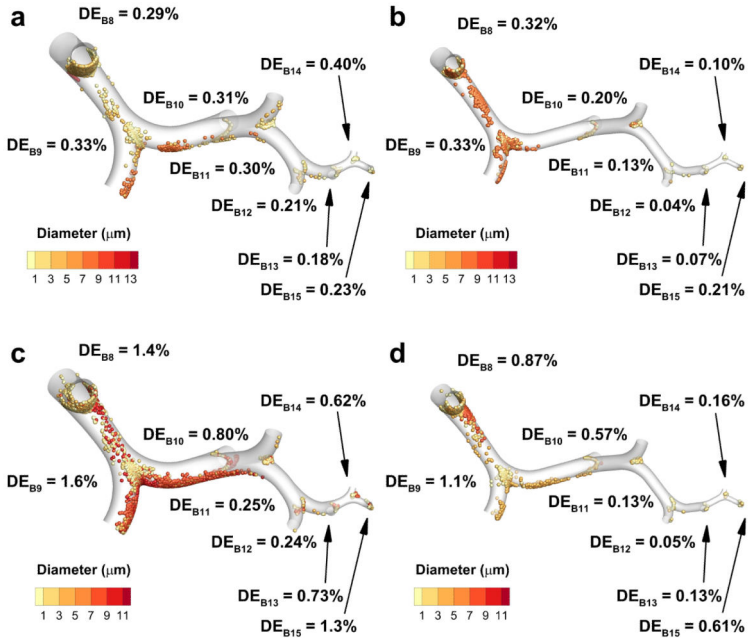

Figure 5.

Deposition efficiency (DE) estimates based on CFD predictions for the eighth through the fifteenth bifurcations (B8-B15) of the left lower (LL) lobe stochastic individual path (SIP) model. The cases presented are for non-constricted and constricted airways with metered dose inhaler (MDI) delivery (a and b) and with dry powder inhaler (DPI) delivery (c and d).

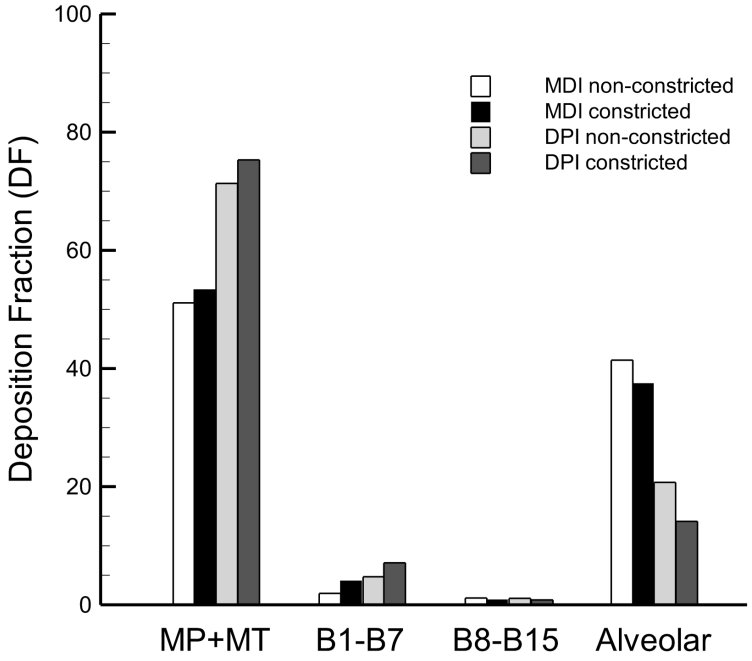

Figure 6.

Deposition fraction (DF) predictions (percentage of aerosolized drug mass) in the mouthpiece plus the mouth-throat (MP+MT), the upper and middle tracheobronchial (TB) (B1-B7), lower TB (B8-B15), and alveolar regions for all four cases.

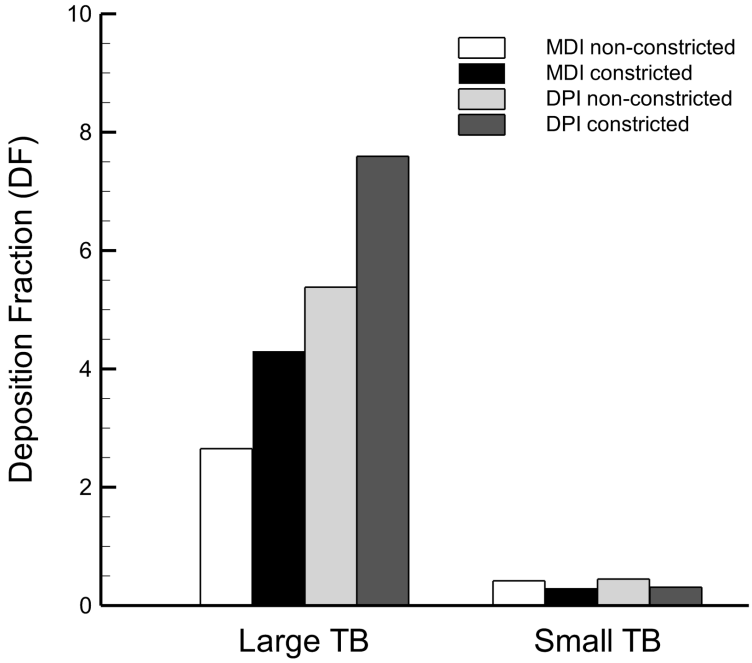

Figure 7.

Deposition fraction (DF) predictions (percentage of aerosolized drug mass) in the large (> 2 mm diameter) and small (< 2 mm diameter) tracheobronchial (TB) airways.

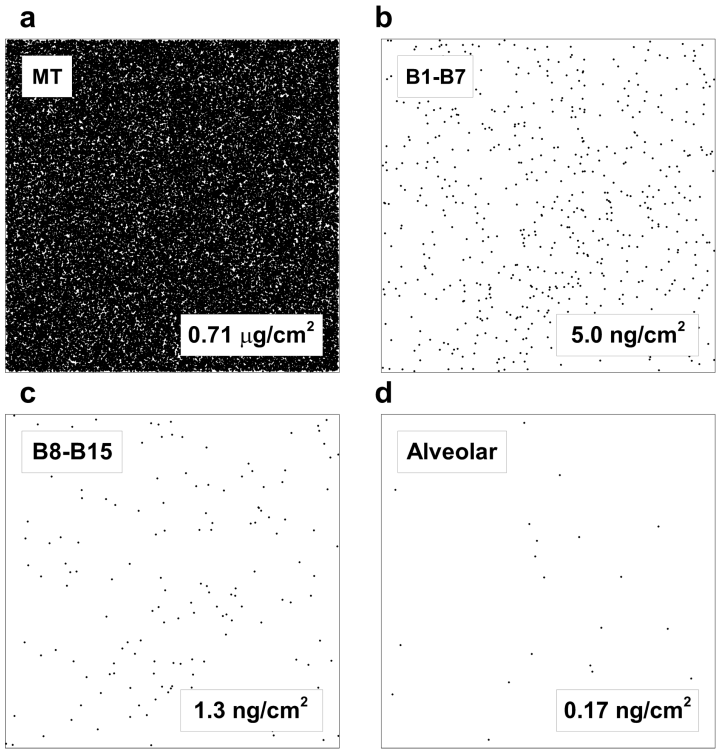

Figure 8.

Representation of deposited particle number density on 1 cm^2 lung surface tissue samples taken from the (a) extrathoracic, (b) upper and middle tracheobronchial (TB) (B1-B7), (c) lower TB (B8-B15), and (d) alveolar regions. An initial aerosol dose of 250 μg fluticasone propionate was assumed to consist of monodisperse 2.64 μm particles with DF values based on the non-constricted MDI results. The number of particles that would deposit on a 1 cm^2 tissue sample in each region is shown. The drug dose that would be delivered to each 1 cm^2 tissue sample is also reported.

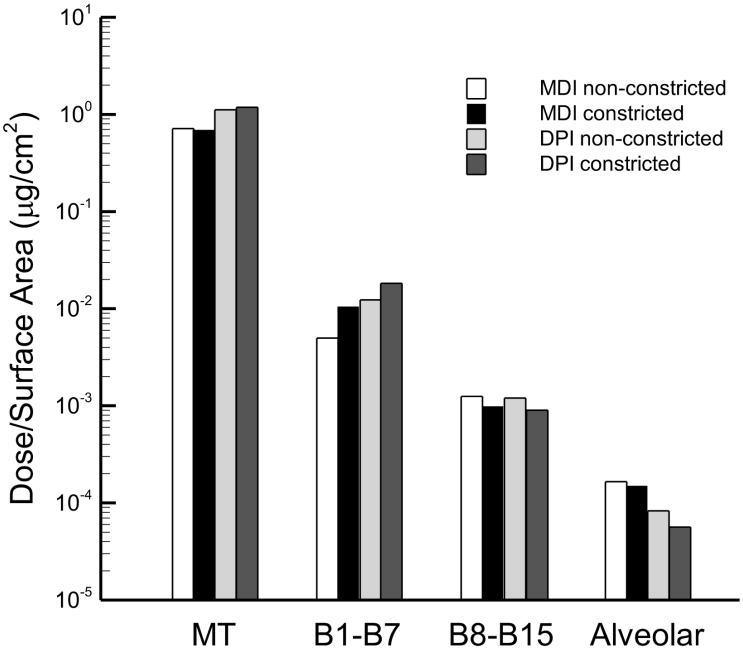

Figure 9.

Concentration of drug mass per unit of surface area (μg/cm^2) based on an aerosolized fluticasone proprionate dose of 250 μg evaluated within the mouth-throat (MT), the upper and middle tracheobronchial (TB) (B1-B7), lower TB (B8-B15), and alveolar regions.

Table 1

Average bifurcation diameter (given in mm) from the fourth bifurcation (B4) to the fifteenth bifurcation (B15) for the non-constricted and inflammation constricted pathways in the five SIP models: left lower (LL), left upper (LU), right lower (RL), right middle (RM), and right upper right (RU). Diameter measurements in the non-constricted pathways are based on scaling data in the RL lobe from Yeh and Schum[19] to a lung volume of 3.5 L.

	Non-Constricted					Constricted				
Bifurcation	**LL**	**LU**	**RL**	**RM**	**RU**	**LL**	**LU**	**RL**	**RM**	**RU**
B4	7.38	7.14	8.64	6.16	6.50	5.42	5.00	6.04	4.31	4.55
B5	6.13	5.65	6.84	4.88	5.15	4.29	3.96	4.79	3.41	3.60
B6	4.98	4.60	5.56	3.96	4.18	3.49	3.22	3.89	2.77	2.93
B7	4.46	4.12	4.98	3.55	3.75	3.12	2.88	3.49	2.49	2.62
B8	3.61	3.33	4.03	2.87	3.03	2.53	2.33	2.82	2.01	2.12
B9	2.81	2.60	3.14	2.24	2.36	1.97	1.82	2.20	1.57	1.65
B10	2.66	2.46	2.97	2.12	2.23	1.86	1.72	2.08	1.48	1.56
B11	2.43	2.24	2.71	1.93	2.04	1.70	1.57	1.90	1.35	1.43
B12	1.91	1.76	2.13	1.52	1.60	1.34	1.23	1.49	1.06	1.12
B13	1.39	1.28	1.55	1.10	1.17	0.97	0.90	1.09	0.77	0.82
B14	1.03	0.95	1.15	0.82	0.87	0.72	0.67	0.81	0.57	0.61
B15	0.77	0.71	0.86	0.61	0.65	0.54	0.50	0.60	0.43	0.45

J Pharm Sci. Author manuscript; available in PMC 2017 January 13.

Table 2

Normalized distribution of particle mass at B4 inlets of the five SIP models for MDI and DPI cases in non-constricted and constricted geometries based on transport through the upper TB models. The mass values of each case are normalized using the average mass entering the five lung lobes.

	MDI		DPI	
Lobe	**Non-Constricted**	**Constricted**	**Non-Constricted**	**Constricted**
LL	1.332	1.010	1.316	1.308
LU	1.066	1.130	1.051	1.032
RL	1.154	1.079	1.274	1.245
RM	0.366	0.395	0.361	0.365
RU	1.082	1.386	0.997	1.050

Table 3

Deposition fraction (DF) values (given as a % of aerosolized dose) in the B4-B7, B8-B15 and B4-B15 regions for all cases. The values of DF in each region are the summation of results from all five lobes.

		Deposition Fraction (% of Aerosolized Dose)		
		B4-B7	**B8-B15**	**B4-B15**
MDI	**Non-constricted**	0.73	1.13	1.86
	Constricted	1.40	0.89	2.29
DPI	**Non-constricted**	1.85	1.08	2.93
	Constricted	1.38	0.81	2.19